UiT The Arctic University of Norway

AMB – Department of arctic and marine biology

Estimating secondary production and egg production of *Calanus spp.* at the Polar front

Torkel Granaas

Master's thesis in biology - BIO-3950 - May 2023

Acknowledgements

I want to express my gratitude to my supervisor Sünnje Linnéa Basedow for giving me the opportunity to work on this thesis. I'm very thankful for her help throughout the process, and without her knowledge, experience and understanding of the subject matter, writing this thesis would not have been possible. It has been a huge learning experience for me, and I have been lucky to be able to write a thesis on a truly fascinating topic. I'm grateful for the help from Malin Daase during the egg production experiments and sampling overall. Thanks to Emilia Trudnowska who together with Sünnje deployed the LOPC and different stations. Thanks to Rolf Gradinger for his leadership at the Polar Front cruise, and thanks to the crew at RV Helmer Hansen for being helpful during the cruise. And lastly, I'm thankful for my friends and classmates for the great company and thoughtful discussions about biology and other topics throughout the last years.

Abstract

The Barents Sea Polar Front is a biological hotspot, as the ice edge bloom happens in close proximity to the front, while on the Atlantic side advection carries plankton towards the front. It is of great interest to learn more about zooplankton secondary production in the region, as this gives an indication of how much energy is available for higher trophic levels. Secondary production and egg production of *Calanus spp.* was estimated across two transects on the Atlantic side of the Barents Sea Polar Front during the spring bloom. The sampling was done semi-automatic, with towed instrument packages recording amongst other zooplankton biovolume with the LOPC, fluorescence and temperature. This in turn was used to compute growth rates using a semi-empirical formula, which were applied to the observed biomass of zooplankton. In addition, biovolume spectrum was constructed to further understand the state and size structure of the zooplankton community. At different stations female *Calanus spp.* were collected to measure egg production rate, which in combination with abundance counts from the LOPC gave estimates of *Calanus* egg production across the transects. Secondary production in the upper 50 meters of the water column was estimated to be on average 5 and 6 mg carbon m^{-3} day^{-1} across the first and second transect, respectively. Contribution of egg production to total secondary production was highest on the second transect, but the method could be prone to overestimation of egg production. The biovolume spectra indicated productive zooplankton communities typical for a spring bloom scenario. This study demonstrates the strengths of using semi-automatic sampling to discover spatial patterns in zooplankton secondary production.

Table of Contents

1 Introduction

The Polar Front is an area of high productivity and importance for the ecosystem in the Barents Sea (Basedow, Zhou, & Tande, 2014). Warmer, more saline Atlantic water meets the colder Arctic water at the Polar Front (Våge, Basedow, Tande, & Zhou, 2014). Several factors contribute to the high productivity of the polar front; zooplankton are brought by advection from the south, some further north than the range in which they normally inhabit. In the spring, the ice edge is located not far from the polar front, and as the ice melts here, stratification makes it possible for a spring bloom of phytoplankton to start early, compared to the bloom in the open waters (Wassmann et al., 1999). The species *Calanus finmarchicus* and *Calanus glacialis* plays a key role in the ecosystem as they graze on phytoplankton, enabling energy from primary production to travel to higher trophic levels in the form of nutrient rich lipids (Falk-Petersen, Mayzaud, Kattner, & Sargent, 2009). For example, nauplii of *C. finmarchicus* are an important prey item for fish larvae, and planktivorous fish such as capelin (*Mallotus villosus*) and polar cod (*Boreogadus saida*) rely heavily on lipid rich stages of *Calanus* as a food source (Aune et al., 2021; Orlova et al., 2010).

In the last decades, semi-automatic optical based sampling technology have been developed, increasing the spatial resolution of zooplankton sampling (Basedow, Tande, Norrbin, & Kristiansen, 2013; Espinasse et al., 2018). Theoretical advancements have also been made, resulting in biomass spectrum theory, optimized to work with data obtained from optical sampling methods, which can be used to draw inferences about the state of the zooplankton community (Zhou, 2006; Zhou & Huntley, 1997). As the Polar Front is a biological hotspot in the Barents Sea, it is of great interest to learn more about the zooplankton community in this region, and estimates of secondary production based on optical sampling methods might contribute to our understanding of the Barents Sea Polar Front.

1.1 Barents Sea Polar Front

The Barents Sea is a shallow sub-Arctic shelf sea, and a very productive region (Reigstad et al., 2002). The hydrography is characterized by inflow of Atlantic water from the southwest, and Arctic water from the north (Våge et al., 2014). The Polar Front is the area where the Atlantic water (AW) meets Arctic water (ArW), and the position of the front in the western part of the Barents Sea is connected to Southern flank of the Spitsbergen Bank, following the shelf slope. While in the eastern region of the Barents Sea the location of the front varies more (Våge et al., 2014). The AW is characterized by being warmer and more saline than the ArW, as such there is a gradient of salinity and temperature across the front, but not density. Both lower temperature and higher salinity makes the water denser, this results in making the Polar Front density compensated (Fer & Drinkwater, 2014), which limits vertical flows. The Polar Front forms a barrier preventing the marginal ice zone (MIZ) to expand further south (Barton, Lenn, & Lique, 2018).

Sea surface temperature of the Barents Sea have increased in the last years, resulting in a decrease in seasonal sea ice coverage and a longer growing season for phytoplankton in the northernmost regions, causing an increase in primary production (Dalpadado et al., 2014). The increase in sea surface temperature is most likely a result of inflow of AW with higher temperature than before (Barton et al., 2018). A continued rise in sea surface temperature, mediated by global warming, is documented to have caused the establishment of boreal species further north into the Arctic in recent times (Kortsch et al., 2015).

While the first phytoplankton bloom in the Barents Sea starts in the south, another bloom starts at the Polar front at the border of the MIZ (Wassmann et al., 1999). The bloom at the Polar Front is able to start so early because of the stratification of the water masses, a lid of relatively fresh water from the melting of sea ice (Daase, Berge, Søreide, & Falk-Petersen, 2021). This stratification holds nutrients, and the bloom at the MIZ happens in a short burst, and as nutrients are depleted and MIZ retreats, the phytoplankton bloom moves northwards (Wassmann et al., 1999). There is also an ice algae bloom occurring under and in the sea ice, before the main bloom, and in the northern Barents Sea it might contribute as much as 20% of total primary production (Hegseth, 1998). The stratification of water masses happening at the

Arctic side of the polar front limits vertical mixing and thus also nutrient supply (Daase et al., 2021), but in the Atlantic influenced region of the Barents Sea mixing is more prevalent sustaining a longer phytoplankton bloom (Reigstad et al., 2002).

1.2 Zooplankton community at the Polar Front

1.2.1 Life cycle and biology of *Calanus spp.*

Calanus finmarchicus (*C. finmarchicus*) and *Calanus glacialis* (*C. glacialis*) are copepods, and important grazers in the Barents Sea, making up a substantial part of the mesozooplankton biomass in the region (Falk-Petersen et al., 2009). *C. finmarchicus* is distribution is further south than the sub-Arctic species *C. glacialis*, that mostly inhabit the shelf regions north of the polar front, most of which are seasonally ice covered (Falk-Petersen et al., 2009). Although *Calanus* is mainly herbivorous, during post-bloom periods it can switch to being omnivorous, getting substantial amounts of energy from microzooplankton (Campbell et al., 2009; Ohman & Runge, 1994). As an adaptation to the highly seasonal environment they inhabit, both species undergo seasonal vertical migration in the end of the season, descending in the water column and entering diapause, before emerging at the surface late winter, to graze on the seasonal phytoplankton bloom that occurs in spring, and reproduce (Falk-Petersen et al., 2009). *Calanus* has six nauplii stages, and five copepodite stages (CI-CV) before becoming adults. *Calanus* accumulate lipids during the spring and summer, and it is these large lipid stores that makes overwintering possible (Falk-Petersen et al., 2009).

C. finmarchicus has a lifecycle of 1 year in its northernmost range of distribution, starting its life as a nauplii after hatching during or after the spring bloom, developing from nauplii to copepodite stages (Falk-Petersen et al., 2009). Although it has been debated how important local production is to replenish the population (Kvile, Fiksen, Prokopchuk, & Opdal, 2017), advection from the Norwegian Sea plays a crucial role in replenishing the *C. finmarchicus* stock in the Barents Sea (Skaret et al., 2014). During the later copepodite stages *C. finmarchicus* stores energy in lipid sacks, before overwintering as mostly CV copepodite stage (but also CIV), developing into the last stage during winter. *C. finmarchicus* is an

income breeder, meaning it relies upon energy from grazing to produce eggs (Hatlebakk, Kosobokova, Daase, & Søreide, 2022). As lower water temperatures slow down growth and development, life cycles of the copepods generally become longer at higher latitudes. Further south, in the North Sea *C. finmarchicus* can have up to 3 generations per season in (Falk-Petersen et al., 2009).

C. glacialis has a one or two year life cycle, and can either overwinter as a CIV, emerge from dormancy, and spend another season accumulating lipids, and then overwintering a second time before reproducing, or have a 1-year life cycle similar to *C. finmarchicus* (Falk-Petersen et al., 2009). *C. glacialis* is on average larger than its Atlantic counterpart, and is a mix of income and capital breeder, meaning it uses both energy from stored lipids and grazing to produce eggs. As such, it can start spawning before the spring bloom, possible fuelled by ice algae as well (Falk-Petersen et al., 2009). The larger lipid stores and size is an adaptation to an environment where the spring bloom is less predictable than in regions without sea ice cover, and the plasticity in life history strategy of *C. glacialis* allows for slower lifecycle in a region with unpredictable and short phytoplankton blooms, or a 1 year lifecycle under very favourable conditions (Falk-Petersen et al., 2009; Hatlebakk et al., 2022). It should be mentioned that research based on molecular analysis suggest that morphological traits such as size and pigmentation are unreliable in distinguishing *C. glacialis* and *C. finmarchicus* from each other, suggesting that species misidentification could have been widespread (Choquet et al., 2018).

Nauplii of *C. finmarchicus* is important food for fish larvae, and for many planktivorous fish lipid rich *Calanus* is a substantial part of their diet. Therefore, *Calanus spp.* play an important role as a trophic link for energy to flow from primary producers to planktivorous fish species, and these forage fish in turn are the main prey for cod (*Gadus morhua*), seabirds and marine mammals (Dalpadado et al., 2014).

1.2.2 Zooplankton diversity at the Polar Front

There are many smaller species of copepods besides *Calanus spp*. at the Polar Front as well, and these species usually have a higher numerical abundance than *Calanus* (Aarflot, Skjoldal, Dalpadado, & Skern-Mauritzen, 2018; Daase et al., 2021). Some of the smaller copepods are omnivorous and opportunistic feeders, such as *Oithona similis, Triconia borealis* and *Microcalanus spp.,* while *Pseucocalanus spp.* is mainly herbivorous (Daase et al., 2021). Common to the smaller species of copepods is that they do not have large enough stores of energy to undergo diapause, and thus need to feed sporadically throughout the winter, although some species show patterns of weak seasonal migration (Daase et al., 2021). Other important species of zooplankton include euphausiids, such as *Thysanoessa inermis,* which are predominantly herbivorous but supplement with omnivorous diet during winter (Dalpadado, Yamaguchi, Ellertsen, & Johannessen, 2008). Together with *Calanus spp.,* euphausiids are an important food sources for higher trophic levels in the Barents Sea (Dalpadado et al., 2014). Many other taxa of zooplankton also appear in the region, such as amphipods, pteropods, ctenophores, chaetognaths and appendicularians (Daase et al., 2021).

1.2.3 Microbial food web

Although the grazing of copepods on phytoplankton are important in the Barents Sea food web, the microbial part of the food web should not be overlooked. After a short productive spring bloom, the nutrients in the upper water masses are mostly depleted. This nutrient poor environment during the post bloom period, where primary production is primarily based on remineralized nutrients, favours phytoplankton species with small cell sizes, such as autotrophic flagellates (Daase et al., 2021). In addition, heterotrophic bacteria utilize dissolved organic carbon from dead organism, fecal pellets and particles from inefficient feeding. Heterotrophic flagellates consume both heterotrophic bacteria and autotrophic flagellates, witch in turn are consumed by protozooplankton such as ciliates and dinoflagellates, which again are consumed by copepods (Daase et al., 2021). It has been hypothesized that increasing ice melt and freshwater input into the Arctic could enhance

stratification, and thus make favourable conditions for autotrophic flagellates, funnelling more energy through the microbial loop, witch would mean less energy available for higher trophic levels (Vincent, 2010). Another effect of increased microbial activity could be higher retention of carbon in the pelagic ecosystem decreasing loss to the benthos (Franzè & Lavrentyev, 2017).

1.3 Biomass spectrum theory

Biomass spectrum theory is a method of modelling pelagic ecosystems, often focusing on zooplankton, by organising organisms according to size rather than species or functional groups. Biomass spectrum theory describe energy flows through size classes in the ecosystems, and inferences about community productivity, mortality, growth and trophic levels can be made based on the biomass spectrum (Zhou, 2006; Zhou & Huntley, 1997).

Biomass spectrum theories builds upon Sheldon's size spectrum, which display a pattern of how organisms are organized by mass in the marine ecosystem. By organising organism into logarithmic body mass bins, that are linear on the log scale, and measuring total biomass contained in each bin, it was found that the biomass contained within each bin was roughly equal (Blanchard et al., 2017; Sheldon, Prakash, & Sutcliffe Jr, 1972). It follows then, that abundance of individuals declines from smaller to larger body mass bin, as each size bin has equal biomass but organism size increases (See Figure 1).

Platt and Denman (1977) introduced the normalized biomass spectrum, where biomass in each bin was divided by the linear width of the size interval, and the normalized biomass and size interval log transformed. When fitting a linear regression with size interval as predictor variable, and the normalized biomass as response variable, both on the logarithmic scale, it follows mathematically that the slope should be around -1, assuming roughly equal biomass within each bin (Sprules & Barth, 2016). Later Zhou and Huntley (1997) formulated a mathematical theory of zooplankton population dynamics based on the normalized biomass spectrum, and Zhou (2006) built upon this demonstrating how parameters such as growth rates, trophic levels and abundance change could be calculated from the slope of the normalized biomass spectrum (referred to as the 'biomass spectrum' from now on). By

dividing the biovolume by the length of the size interval (normalizing), we ensure that the biomass spectrum is independent from how the chosen length of the intervals (Zhou, 2006), and comparisons can be made between spectra constructed with different size classes (Sprules & Barth, 2016).

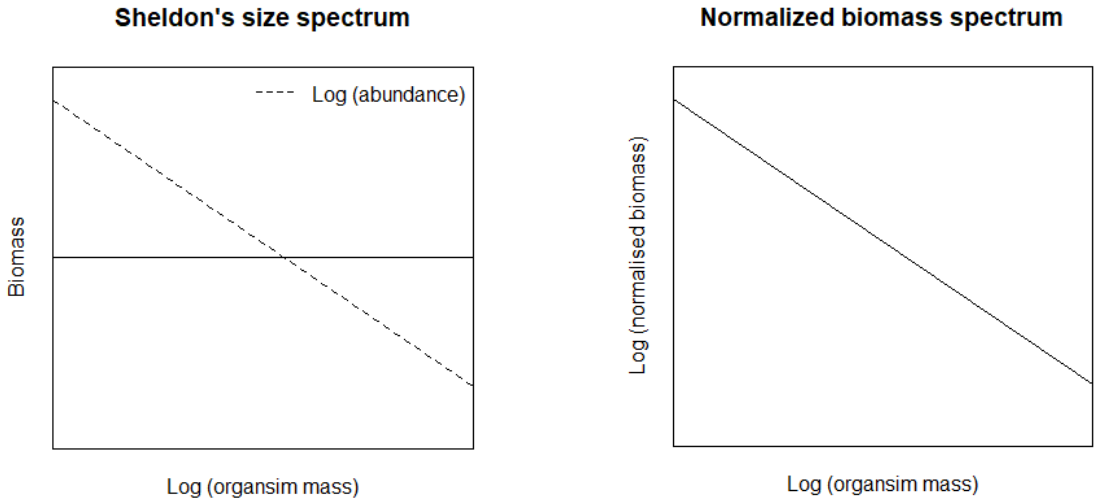

Figure 1: Sheldon's size spectrum (left) and the normalized biomass spectrum (right). Stippled on Sheldon's size spectrum indicating log(abundance), while the solid line indicates biomass.

One of the main motivations for the development of size spectrum theories, is that sampling can then be done semi-automatic, on a much larger spatial scale than traditional net sampling of zooplankton allows (Platt & Denman, 1977; Zhou, 2006). The challenge when using nets to sample zooplankton communities, is that mesozooplankton have a patchy distribution, meaning that net sampling might be prone to over or underestimating plankton abundances, due to working on a small spatial scale (Espinasse et al., 2018; Zhou, Tande, Zhu, & Basedow, 2009).

In the last decades new technology has improved the spatial resolution of sampling, namely with the optical plankton counter (OPC) and later the laser optical plankton counter (LOPC). The latter is an improvement upon its predecessor, reducing the number of coincidental counts (several particles counted as one) and has a much better capacity in terms of amount of water volume sampled and how high density of particles it can operate in (Herman, Beanlands, & Phillips, 2004). Sampling an equivalent size range of organisms with nets would require several mesh sizes to be used. However, the LOPC have no taxonomic resolution, so nets or video plankton recorder are needed to know the species composition of

the zooplankton community (Basedow et al., 2013). As the LOPC measures volume, spectra will be based on volume measurements rather than mass. Biovolume spectra are analogous to biomass spectra (Basedow, Tande, & Zhou, 2010), but some researchers have found that slopes obtained from biomass spectra are significantly steeper than that of biovolume spectra (Atkinson et al., 2021), as such slopes and intercepts derived from spectra using different units should not be directly compared.

Another argument for a size-based approach to model the ecosystem, is that the zooplankton community is incredibly complex. Drawing trophic links between species and/or functional groups is a challenging task, especially as individuals of the same species might have a completely different diet based on food availability, varying a lot over small changes in space and time (Zhou, 2006; Zhou, Carlotti, & Zhu, 2010). While predator prey relations between taxonomic groups are far from constant, the zooplankton community is very size structured, and the biomass spectra of this community is mostly linear, allowing the use of biovolume spectrum theory. The size of an organism can be looked upon as a master trait, determining metabolism, growth and respiration, so an approach that mainly uses organism size will be useful for explaining fluxes of biomass through the ecosystem (Blanchard et al., 2017).

1.3.1 Interpreting the slope and intercept of a biovolume spectrum

According to Zhou (2006), the slope and intercept of the biomass spectrum represents inherent properties of the community: When the intercept is high, a lot of small organisms have entered the spectrum, thus the primary production is high. A steep slope of the biomass spectrum indicates a productive community dominated by grazers and predators, with high mortality and efficient energy transfer to bigger size classes (Zhou, 2006). A flat slope indicates a community with lots of recycling of mass, and a food web dominated by omnivores and carnivores, and with many trophic levels. If we assume a constant assimilation efficiency, biomass would need to be recycled to maintain the high biomass present in the biggest classes when we have a flat slope (Zhou, 2006).

Other researchers argue for a different interpretation of the slope of a biomass spectrum. Assuming a constant predator-prey mass ratio (PPMR), the steeper the slope is, the less energy (mass) is transferred from the smallest organisms to the lowest, thus indicating low trophic transfer efficiency (Atkinson et al., 2021; Mehner et al., 2018). Zhou (2006) argues that assuming a constant PPMR isn't valid for the zooplankton community, and empirical evidence has been found supporting Zhou's hypothesized relationship between the state of the community and slope of the biovolume spectra (Giering et al., 2019; Zhou et al., 2009). Thus, biovolume spectrum theory would predict steep slopes from spectra sampled during the phytoplankton bloom, while communities sampled during a post-bloom period or during winter are predicted to have flat slopes.

1.4 Estimating growth rate and secondary production

Secondary production in the pelagic zone determines how much food is available to species higher in the food web, and it is therefore of great interest to obtain estimates of secondary production in the Barents Sea (Basedow et al., 2014; Dalpadado et al., 2014). Many different methods have been used to estimate secondary production of zooplankton, such as the ecological method, the cohort method, the physiological method, radiochemical methods, and the growth rate approach (Poulet, Ianora, Laabir, & Breteler, 1995; Runge & Roff, 2000). The growth rate approach consists of making measurements of growth rates for different stages of copepods, multiplying growth rates with biomass for the respective stages, and summing up for all stages to get estimates of secondary production (Poulet et al., 1995). The challenge with the growth rate approach is that if *in situ* growth rates where to be measured directly, it would need to be done for each stage for the species in question. This would be laborious, and thus limiting the spatial and temporal scale covered by this method, as well as limiting how many species could be covered (Poulet et al., 1995).

Berggreen, Hansen, and Kiørboe (1988) presented as a more efficient variant of the growth rate approach, simply measuring growth based of egg producing females. Assuming growth rates is equal for egg producing females and juvenile stages, this would yield estimates of secondary production with less sampling required than the original growth rate approach

(Poulet et al., 1995). This approach has been criticized, as the assumption that egg production rate are proportional to growth rates of juvenile copepods have been disproven for many species (Kobari et al., 2019). Realizing the assumption do not hold, Poulet et al. (1995) developed the egg production method, only sampling egg production in adult females, as such the method is meant to represent only a fraction of the zooplankton production.

Due to the patchy distribution of zooplankton, an approach that seeks to uncover spatial patterns in secondary production would benefit from the use of semi-automatic sampling (Basedow et al., 2014). Zhou et al. (2010) developed a semi-empirical formula used in the present study to estimate growth rates, based on empirical and teorethical models on zooplankton growth rates (Hirst & Bunker, 2003; M. Huntley & Boyd, 1984). By a combined theoretical and empirical approach, the equation avoids unrealistic estimates of growth rates for sizes and temperatures where few empirical data are recorded (Zhou et al., 2010). The approach taken in the present thesis is in principle similar to the growth rate approach, but with size classes based on LOPC measurements rather than stages, and the growth rates are applied to all zooplankton the LOPC measures within a given size class. Using semi-empirical formulas for growth rates combined with sampling of biovolume with the LOPC, growth rates and secondary production can be estimated over a large spatial scale (Basedow et al., 2014). A direct measurement of *in situ* growth rate would arguably give a more accurate estimation of growth rates than the semi-empirical formula used, at least for the species and stages measured, for the specific location sampled. But while zooplankton biomass varies over several orders of magnitudes, growth rates vary considerably less (M. E. Huntley & Lopez, 1992). Taking this into consideration, accurate measurements of biomass should be the highest priority in order to accurately estimate secondary production.

1.5 Aims and objectives

The objectives of the present thesis is as follows:

To estimate secondary production of the mesozooplankton community during the spring bloom along a transect crossing the polar front.

Estimate egg production by *Calanus spp.* and compare this to total secondary production. Based on the literature on the mesozooplankton community at the Barents Sea Polar Front this should be a considerable part of total secondary production.

Describe the mesozooplankton community at the polar front using biovolume spectrum theory. Theory would predict steep slopes and high intercepts for communities where spring bloom is ongoing, and flat slopes in more dormant areas.

2 Methods

2.1 Sampling area

The sampling area was the western part of Barents Sea region, across two transects towards the Polar Front, at approximately 29.5°E, from the 18th to 28th May 2022, with the vessel RV Helmer Hanssen.

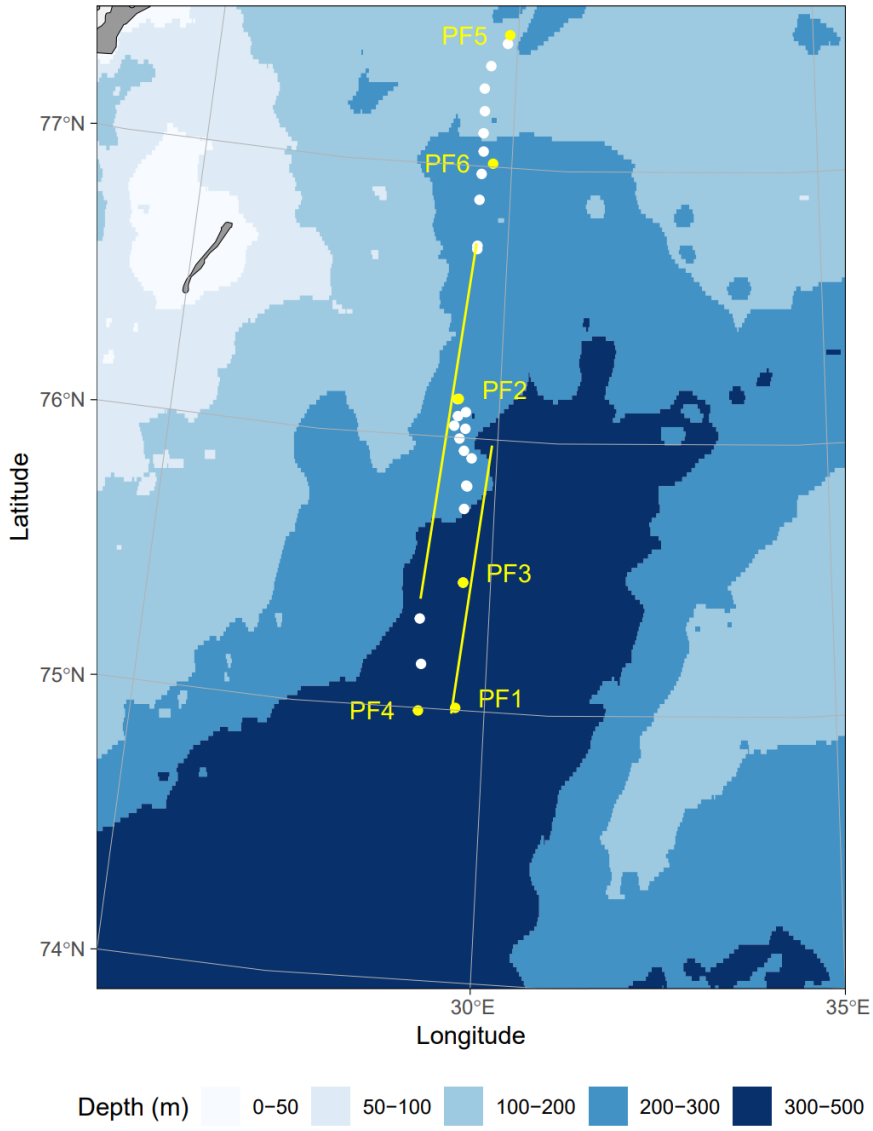

Figure 2: Sampling area, yellow dots indicating stations, yellow lines representing the two transects and white dots indicating VPU profiles. Figure courtesy of S. L. Basedow.

2.2 Sampling of environmental data

To gather environmental data different sensors where mounted on a moving vessel profiler (MVP, ODIM Broke Ocean), see Herman et al. (1998), and a vertical profile unit (VPU). The sensors mounted on the MVP where conductivity-temperature-depth (CTD, Applied Microsystems Micro CTD), fluorometer (WETLabs FLRT Chl a fluorimeter) and laser optical plankton counter (LOPC, ODIM Brooke Ocean), see Herman et al. (2004). The same LOPC was mounted on the rosette frame, but different sensors where mounted: CTD (Seabird 19plusV2) and fluorometer (WETLabs EcoFl). The MVP was used to tow the instrument package along the two transects, while only VPU profiles were done at different stations and when transects were unfeasible, for example when there was sea ice. Only down profiles were used when analysing the LOPC data.

The fluorometer mounted on the MVP was used to measure fluorescence, and filtrations were used to establish a relationship between fluorescence and chlorophyll a (Chl a). 200 ml Seawater was filtrated at different points along the transect, tree samples for each location, and the filters put in approximately 10 mL 90 % acetone, covered in aluminium foil, and placed in a cold and dark room for approximately 24 hours. The measurements were done using the fluorometric acidification method, each sample put in a cuvette, and Chl a was extracted using two drops of 5% HCl and gently mixing of the cuvette, measurements done on the lab-fluorometer before (measuring Chl a and phaeopigments) and after adding the acid (measuring phaeopigments).

2.3 Laser optical plankton counter

In the present study the LOPC was used to count particles and measuring their size. The size range of the particles measured by the LOPC are from 100 µm to around 3 cm in equivalent spherical diameter (ESD). The LOPC works in the following way: A Laser diode produces a beam, that is reflected through a lens, mirror and prism that results in a 1*35 mm light beam passing through a 35 element photodiode (Herman et al., 2004). Particles are then counted

when they pass the detection area. Particles are further divided into single element particles (SEP), and multi element particles (MEP), based upon whether they covered one or several slots in the detection area. SEP are from 100 to 1500 µm, while MEPs are 1500 - 35000 µm ESD. Only the cross-sectional area of SEP area measured, while the shape profiles of MEPs are measured. Using the shape profile of MEPs, ESD can be computed for these particles as well.

In certain environmental conditions, for example estuarine waters or upwelling areas, the data from the LOPC could be unreliable, as the high density of detritus particles can be misread as zooplankton (Espinasse et al., 2018). In addition, attenuation index (AI) was calculated for MEPs, which is a measure of the opaqueness of particles counted (Basedow et al., 2013). When calculating biovolume spectra all MEPs of AI > 0.2 was used, while when calculating secondary production only MEPs of AI > 0.4 was used to ensure only zooplankton was included. Processing of raw data from the LOPC was done by S.L. Basedow (computing biovolume and AI amongst other processes).

2.4 Constructing the biovolume spectrum

The biovolume spectrum is defined as (Zhou, 2006):

$$Biovolume\ spectrum\ (b) = \frac{Biovolume\ (mm^3)\ in\ interval\ \Delta v}{The\ size\ interval\ \Delta v\ (mm^3)} * m^{-3}$$

Equation 1: The biovolume spectrum (Zhou, 2006).

To compute the biovolume spectra, biovolume measurements from the 50 different size classes (see Appendix 1) where normalized following Equation 1. Data from the first transect was divided into Atlantic water (salinity > 34.8) and Arctic influenced water (salinity ≤ 34.8). The mean normalized biovolume (b) for each size class in the different water masses was then calculated. Linear regression was then done, with the log 10 transformed predictor variable and log10 of the mean Biovolume spectrum (b) as response variable. The slope was fitted

only using values from the size classes 0.5-3 mm ESD. The same process was done to compute the biovolume spectra from the different stations, except the division by salinity.

2.5 Calculating weight specific growth rate and production

Calculating growth and production based on biovolume spectra can be done with multiple spectra measured over time, but as data collection from the cruise was done over a spatial and not temporal scale, semi-empirical formulas was used to estimate growth and secondary production. Zhou et al. (2010) developed a formula for calculating weight specific growth rates:

$$g(w,T,C_a) = 0.033\left(\frac{C_a}{C_a + 205e^{-0.125T}}\right)e^{0.09\,T}w^{-0.06}$$

Equation 2: Semi-empirical formula for weight specific growth, from Zhou et al. (2010), equation 19.

Units for formula is as follows: g is in day^{-1}, w is in mg carbon, T: temperature in °C, C_a is in mg Carbon, and is converted with a carbon: chlorophyll a ratio of 50 (Basedow et al., 2014). The middle of each size interval was used to calculate w, assuming a mg carbon: mm^3 ratio of 0.0475 (Gallienne, Robins, & Woodd-Walker, 2001). To calculate production, the following formula was used:

$$P = \sum G_i B_i$$

Equation 3: Production based on Basedow et al. (2014) and Poulet et al. (1995). Without the term dw found in formula 3 from Basedow et al. (2014).

Where P is secondary production in mg C m^{-3} day^{-1}, G is weight specific growth rate (in day^{-1}) in the size class i, B is in mg C in the size class i. The formulas for growth were applied to size classes from 0.25 to 4 mm ESD, for both transects, and multiplied by the biovolume (converted to biomass) in each respective size class for each datapoint.

2.6 Egg production

Egg production experiments was done with *Calanus spp*. females from 6 different stations distributed across two transect near the Polar Front. Sampling of females was done using a WP-3 net (1000 µm mesh, 1 m^2 opening), and usually it was sampled from the bottom to the surface. Wind conditions prevented the use of WP-3 at the last station, as such WP-2 (0.25 m^2 opening, 180 µm mesh) was used instead. The sampling started using just the top 100 meters, but as there was a shortage of *Calanus* females sampling continued from the bottom to ensure there was enough females for the egg production experiments. Using a stereo microscope, female Calanus were selected, from the species *C. finmarchicus*, *C. glacialis* and *C. hyperboreus*. Usually around 20 individuals of the dominant species at the station were picked out, but the availability of females did also put some constraints on how many could be used in the experiments. Ideally the egg incubation experiment should start not long after sampling has been done, as such there was limited time to find *Calanus* females after each sampling. All females were incubated in a cup with a false bottom, filled with filtered seawater tapped at the location of the station. The females were stored at 2° Celsius in darkness for 24 hours, after this the females were separated from the cup containing the eggs. The eggs were counted using a stereo microscope, and egg counts for females that died during the experiments were discarded.

Table a: Sampling of Calanus females for egg incubation experiments.

Station	Date	Sampling depth	Sampling gear
P1	20.05.2022	100 m	WP-3
P2	21.05.2022	260 m	WP-3
P3	22.05.2022	350 m	WP-3
P4	23.05.2022	360 m	WP-3
P5	24.05.2022	190 m	WP-3

P6	25.05.2022	220 m	WP-2

As the data from the egg production experiments where not done quantitatively (female^{-1} instead of m^{-2} or m^{-3}), they were combined with LOPC abundance measurements (AI > 0.4, 1.78 – 2.24 mm ESD) to get estimates off egg production m^{-3}. Egg production was converted to carbon assuming a carbon content of 0.23 µgram egg^{-1} female, but further north than 77.25°N on the transect, a carbon content of 0.44 µgram carbon egg^{-1} was assumed (Hirche & Bohrer, 1987).

2.7 Data analysis and graphical presentation

Data analysis where done using the software Rstudio (R Core Team, 2022), the packages ggplot2 and dplyr was used as well (Wickham, 2016; Wickham, François, Henry, & Müller, 2015). To make the transect plots, data was arranged on a grid with spacing of 10 m on the y-axis and 0.02 decimal degrees latitude (0.04 on the second transect) on the x-axis, and the colour bar indicating mean values of all measurements within the same position on the grid.

3 Results

3.1 Environmental conditions

While ice condition made it unfeasible to cross the Polar front on the first transect, on the second transect barely crossed into the Arctic side of the polar front. There was a surface bloom in the southern part of the transect 2, closer to the front there was a subsurface chlorophyll a maximum (see Figure 3). On the southern side of the polar front, colder less saline (polar front melt water) is evident in the surface layer, while the Arctic side of the polar front is characterized by colder less saline water from the all the way through the water column, forming a gradient in salinity and temperature (see Figure 4 and Figure 5).

Clorophyll a concentrations

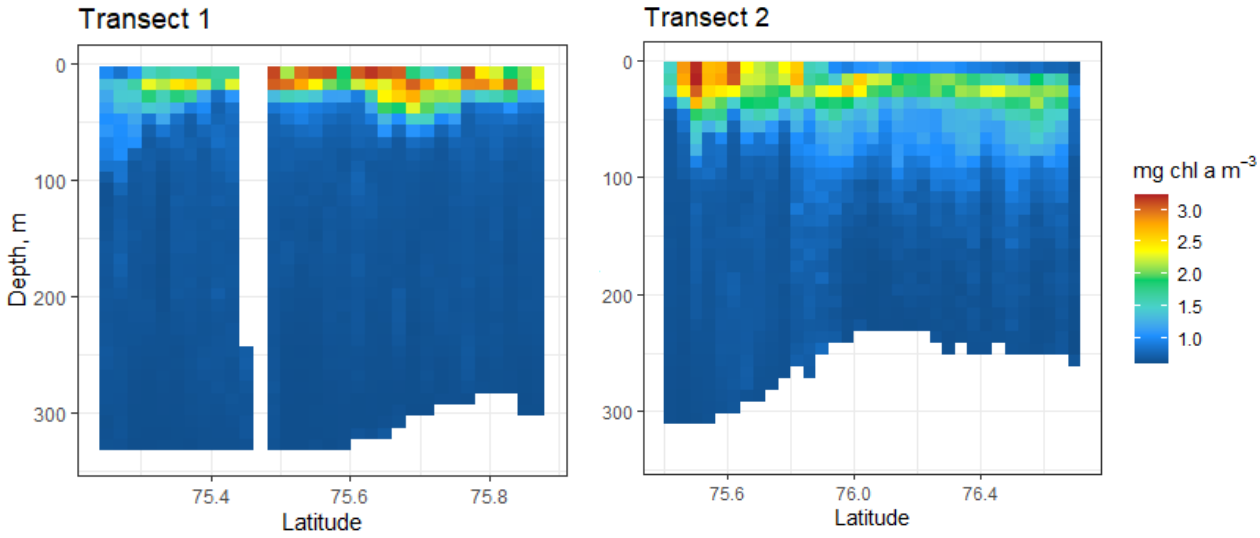

Figure 3: Estimated Chl a concentration based on fluorescence measurements, calibrated with filtration. Colour bar indicating mean chlorophyll a concentration. Showing transect 1 (left), and the second transect (right), VPU excluded from the second transect as the fluorometer was not calibrated. Note the different scales on the x-axis denoting latitude between transect 1 and transect 2 plots.

Salinity

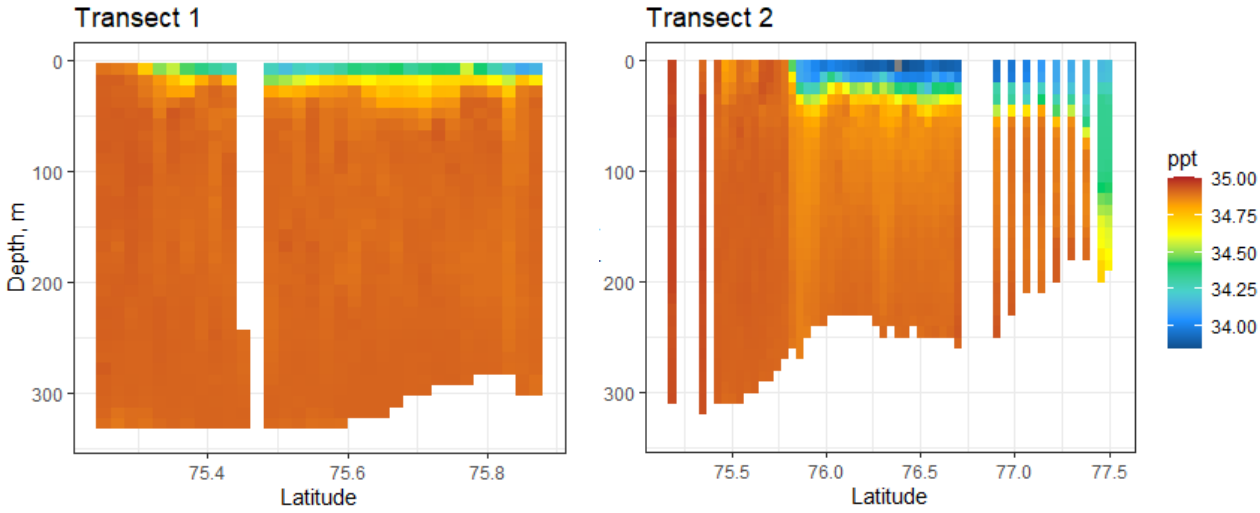

Figure 4: Salinity, measured by CTD for the first transect (left) and second transect (right). Note the different scales on the x-axis showing latitude. Colour bar indicating mean temperature.

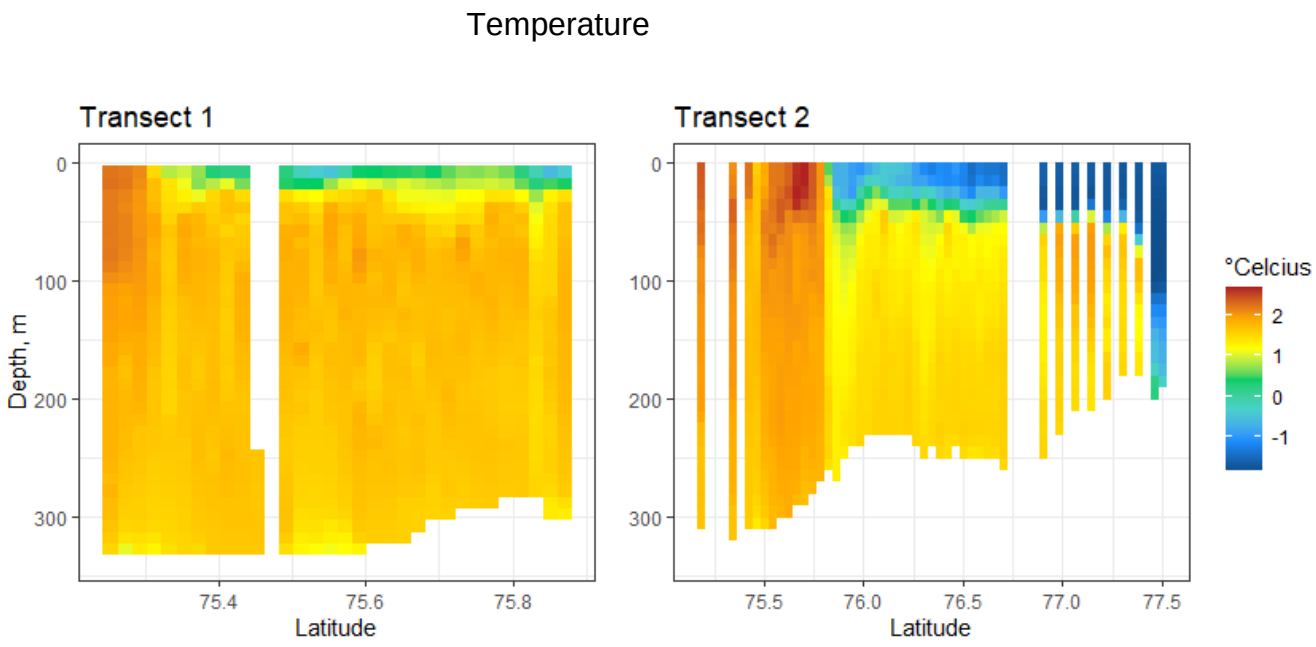

Figure 5: Temperature, for the first transect (left) and second transect (right), colour bar indicating mean temperature.

3.2 Biovolume spectra and zooplankton biomass distribution

3.2.1 Biovolume spectra from transect 1

The biovolume spectra from Atlantic and Arctic water are quite similar: both have and steep slopes (see Figure 6), however the Arctic biovolume spectrum has a higher intercept. Only biovolume spectra from transect 1 where plotted. A dome like shape appeared in the size classes >3 mm ESD on both spectra. See *Table b* for which zooplankton species and stages could inhabit the size spectrum.

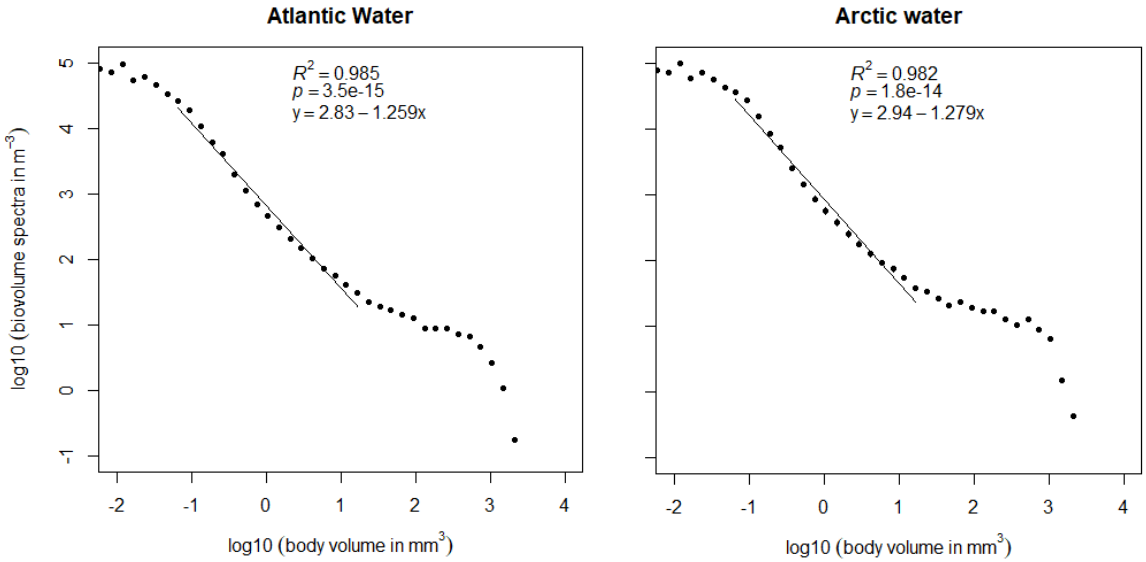

Figure 6: Biovolume spectra from transect, divided into Atlantic water (left) and Arctic influenced Water (right). Log10 of body volume in mm^3 plotted on the x-axis and log10 of biovolume spectra in m^{-3} plotted on the y-axis. Linear regression was fitted using data from particles from 0.5 to 3 mm ESD, and p-value shown is for the slope of the regression.

Table b: Main zooplankton species and which size range they occur in, their estimated ESD and approximate log10(mm^3) as shown on the biovolume spectra plots. Values obtained from Basedow et al. (2010) and Basedow et al. (2014). As the size classes -2.24 ESD was used to calculate egg production, the table was changed to reflect this.

ESD	~log10(mm^3)	Main Zooplankton species and stages:
0.25, 0.6	-2, -1	*Calanus spp.* nauplii, *Oithona spp.*, *Microcalanus spp.*, *Triconia sp.*,
0.6, 1.0	-1, 0	*Calanus spp.* CI-CIII, *Metridia longa*, Chaetognats
1.0, 2.24	-0, 0.6	*Calanus spp.* CIV-CV and adult stages, Chaetognats
<2.24	<0.6	Juvenile and adult Euphasids

3.2.2 Biovolume spectra of stations

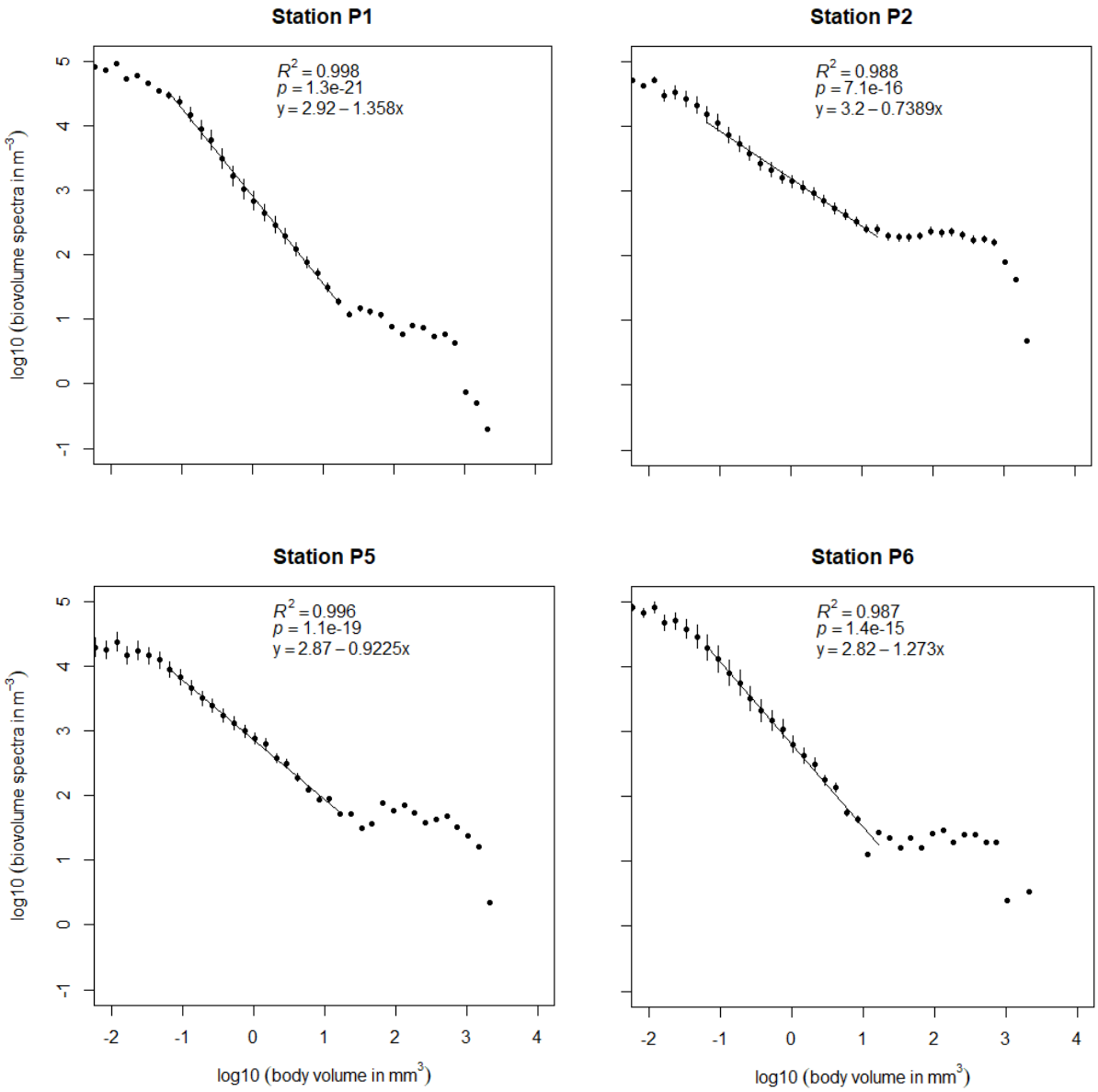

Figure 7: Biovolume spectra from stations P1, P2, P5 and P6. Log10 of body volume in mm^3 plotted on the x-axis and log10 of biovolume spectra in m^{-3} plotted on the y-axis. Linear regression was fitted using data from particles from 0.5 to 3 mm ESD, and p-value shown is for the slope of the regression. As the LOPC was not deployed at station P1, data from the transect was used, from 75.25° – 75.32° North. ± 2 standard errors plotted on each point.

The biovolume spectra from the different stations displayed considerable variation, station P1 and P2 with steep slopes (-1.358 and -1.273 respectively), and station P2 with a flat slope (see Figure 7). Intercepts also varied. Note that biovolume spectra from the different stations is

based on less data than the spectra from the transect, as such there is more uncertainty in the measurements from the stations.

3.2.3 Mesozooplankton biomass distribution measured with LOPC

Biovolume converted to biomass (0.25–4 mm ESD)

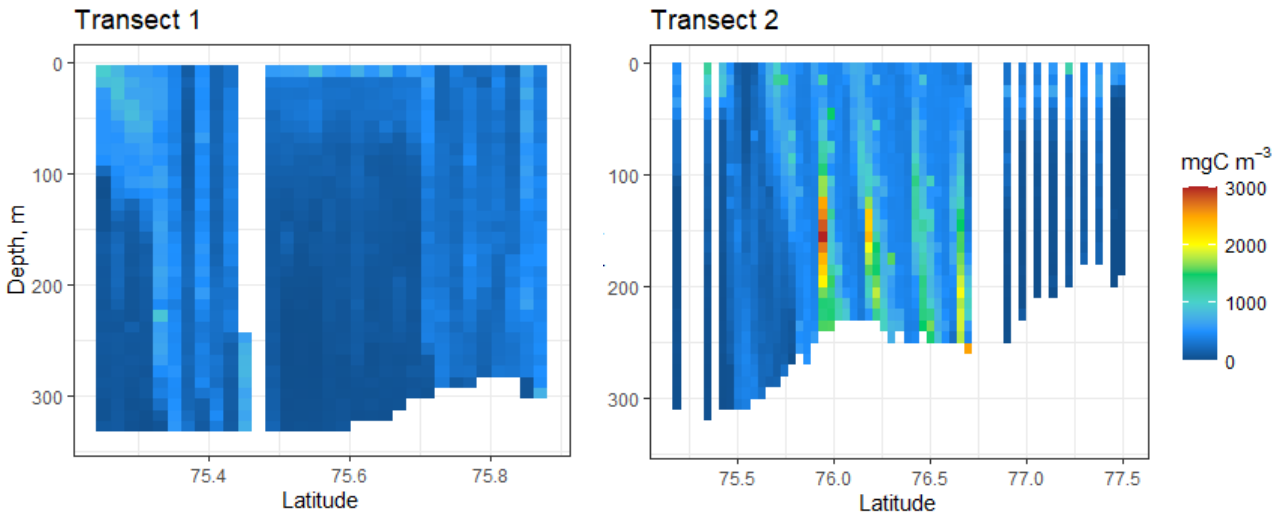

Figure 8: Biomass in mg C m^{-3}, converted from biovolume, measured with the LOPC, within the size range of 0.25-4 mm ESD. Only particles with AI >0.4 to included ensure just zooplankton was measured. First transect on the left, and second transect on the right.

The zooplankton distribution was patchy in both transects, with areas with almost no biovolume measured (see Figure 8), the highest patches of biovolume on transect 1 occurred mostly in the surface, while on the second transect highest patches appeared at 150-200 meters depth.

3.3 Estimation of growth and secondary production

Estimated weight specific growth rate was highest in the uppermost 40 meter, but only reaches around 0.02 day^{-1} on the first transect, and 0.025 day^{-1} on the second transect (see Figure 9). Although growth rates where lower further down the water masses, some estimates indicated a growth rate 0.01 day^{-1} at 200 meter and deeper. The highest estimated secondary production on the first transect occurred in the upper ~50 meters, but there were also patches of low productivity in the surface (see Figure 10). On the second transect patches of quite high productivity occurred further down the water column, around 15-20 mg carbon day^{-1} m^{-3}. Highest production on the second transect occurred in the surface further south on the transect (almost 30 mg carbon day^{-1} m^{-3}, see Figure 10).

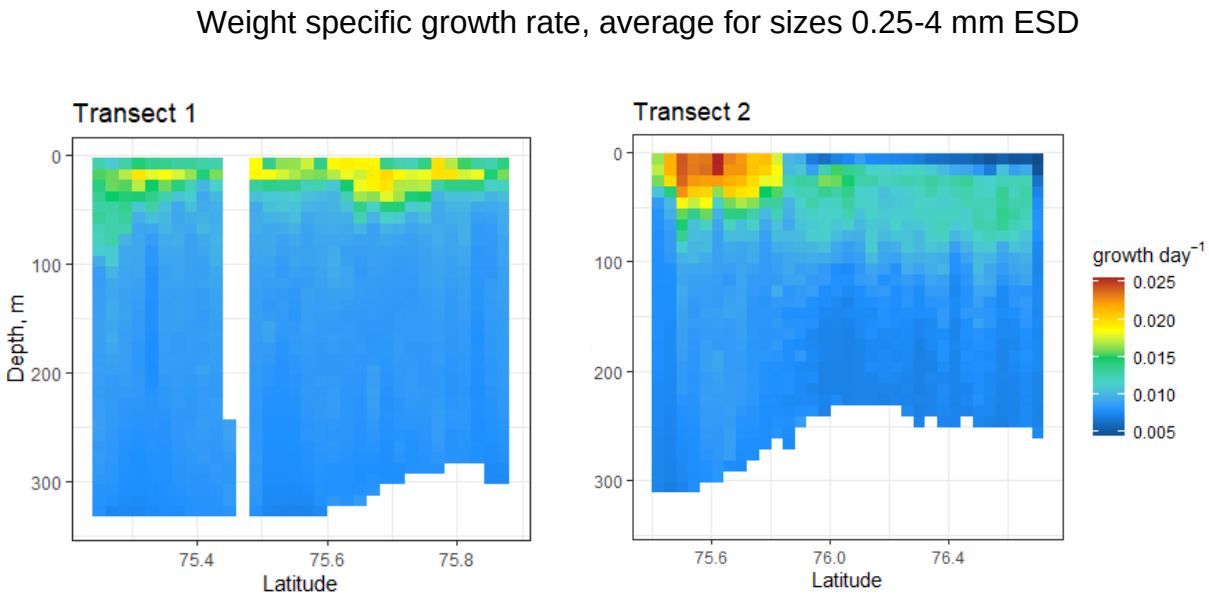

Figure 9: Mean weight specific growth rate of size classes from 0.25 to 4 mm ESD, colour bar indicating growth rate. Transect 1 on the left, transect 2 on the right.

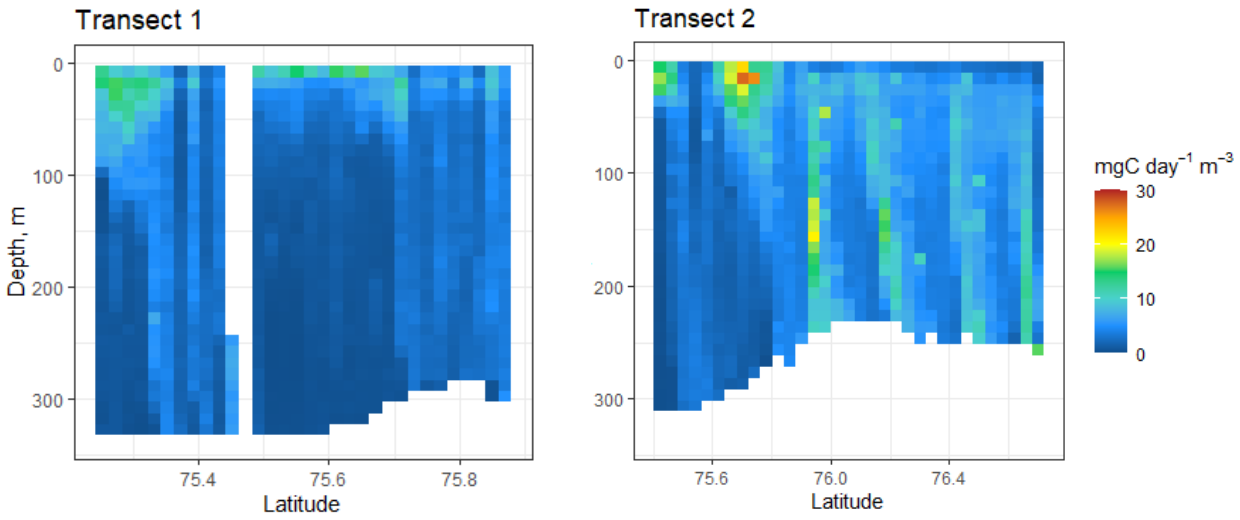

Figure 10: Estimated secondary production in mg carbon day^{-1} m^{-3}, summed up for zooplankton in size classes 0.25-4 mm ESD. Transect 1 on the left, transect 2 on the right. Colour bar indicates secondary production.

3.4 Egg production

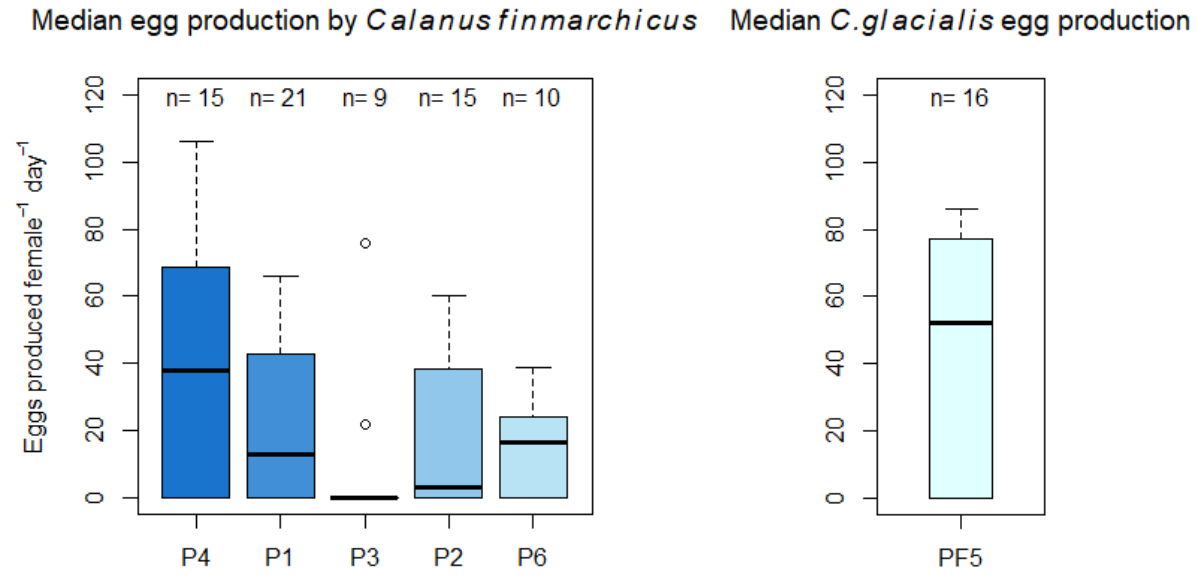

Figure 11: Boxplot of egg production per female day^{-1}, arranged by stations, for C. finmarchicus (left), and C. glacialis (right). Lower side of boxes represent the 1st and 2nd quartile, black bar representing median, and the upper edge of box is the 3rd quartile. Whiskers represent 4th quartile and round dots are outliers, n denotes sample size. Stations are arranged according to latitude, from southernmost at the left of the figure.

There was a lot of variation in egg production among the stations in Atlantic Water (stations P1-P4 and P6, see Figure 11). Most females where *C. finmarchicus*, but at station P5 the majority where *C. glacialis*. *C. glacialis* had a higher median egg production rate than *C. finmarchicus*, but where only sampled adequately at one station. *C. finmarchicus* also appeared in station P5, but most died during the incubation. A considerable number of females produced zero eggs per day, as such 1st and 2nd quartiles are the same for all stations, (see Figure 11). Taking a mean across all Atlantic stations (P1-P4 and P6) gave 21.7 eggs female^{-1} day^{-1}, mean value for P5 was 37.6 female^{-1} day^{-1}. These values were used to calculate egg production m^{-3} day^{-1}, using abundance data from LOPC measurements (see Figure 12).

3.5 Egg production applied to LOPC abundance data

Estimated egg production in mg C day^{-1} was quite patchy, and highest in the 2nd transect (see Figure 12). Egg production by *Calanus spp.* contributed considerably to total secondary production in terms of gram carbon on the second transect (see Figure 13). On the first Transect the egg production was quite low. However, in the northernmost part of the transect, the contribution of eggs was consistently around 10-20% throughout the water column (see Figure 13).

Table c: Summary table for mean secondary production and egg production and their respective standard errors (SE) for transect 1 and 2, divided in upper 50 m and below for each transects, all values in the unit mg C m^{-3} day^{-1} except rightmost column (in %). VPU profiles excluded for transect 2.

	Mean secondary production	SE secondary production	Mean egg production	SE egg production	% egg production
Transect 1 (upper 50 m)	5.35	0.044	0.09	0.006	1.75%
Transect 1 (below 50 m)	2.33	0.021	0.11	0.004	4.66%
Transect 2 (upper 50 m)	6.12	0.075	0.31	0.013	5.05%
Transect 2 (below 50 m)	4.90	0.033	0.69	0.012	13.97%

Estimates of egg production

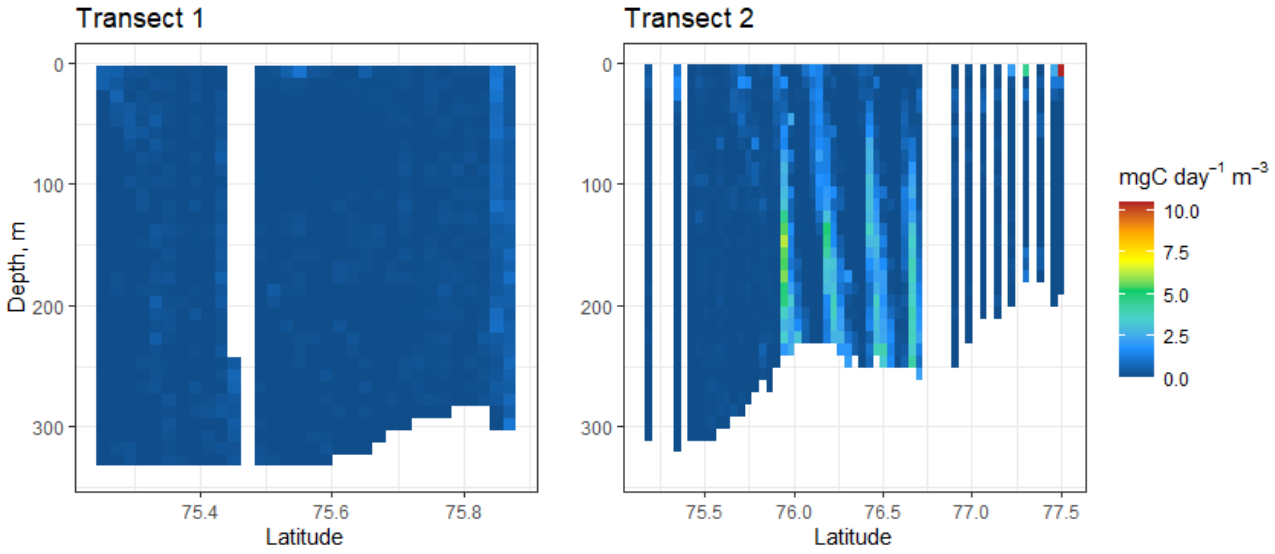

Figure 12: Estimated egg production in mg C day^{-1} m^{-3}, based on LOPC counts of particles of 1.8–2.1 mm ESD and AI of > 0.4, which were assumed to be Calanus spp. females, and average values of egg produced in Atlantic and Arctic influenced waters (21.7 and 37.6 eggs female^{-1}day^{-1} respectively). VPU profiles shown here as estimated is based on abundance counts from the LOPC.

% Egg production of total secundary production

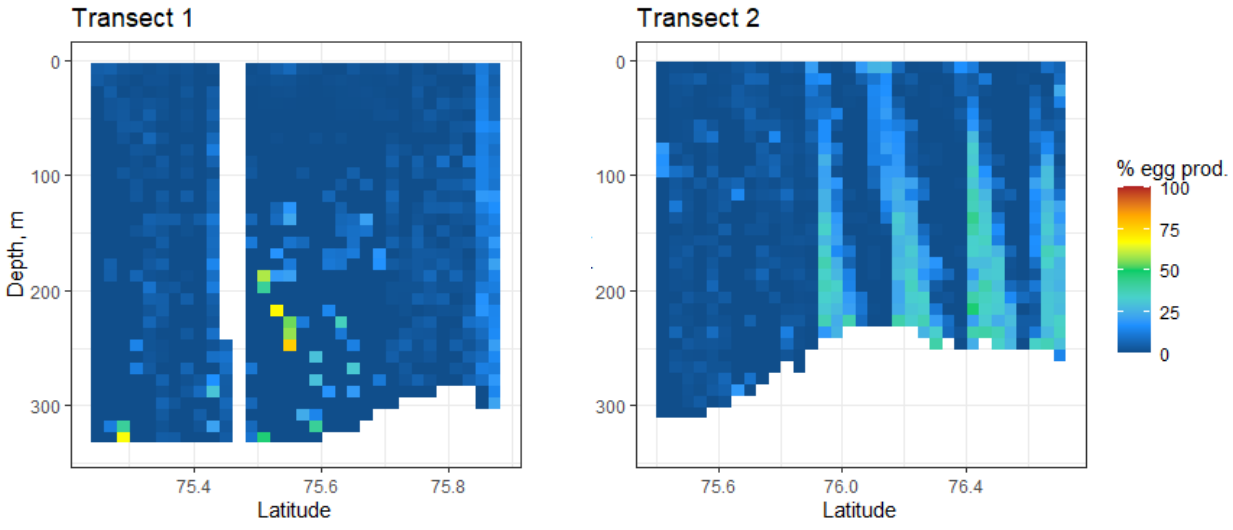

Figure 13: Percentage estimated egg production of total secondary production in carbon, based on Figure 10 and Figure 12.

4 Discussion

4.1 Environmental conditions

The calibration of the fluorometer was not ideal, and half of the calibration measurements were discarded. The formula for the regression used as the relationship between fluorescence and Chl a concentration (see Appendix 2), could overestimate Chl a concentration in area with low fluorescence, such as deep water, and underestimate Chl a in areas with high fluorescence. This would have implications for growth rates and estimates of secondary production. Forcing a regression through origin could been attempted in order to obtain more realistic concentrations of Chl a. The fluorometer mounted on the VPU was not calibrated, thus calculations made based on Chl a concentrations, such as weight specific growth rate and secondary production, were not valid for the VPU profiles for south and north of the second transect. This means that unfortunately estimates of secondary production and weigh specific growth rate were restricted to the Atlantic side of the Polar Front.

4.2 Biovolume spectra

The intercepts and slopes of the biovolume spectra are consistent with another study done in the same region and season (Basedow et al., 2010). The biovolume spectra from transect 1 displayed considerably less variation than the spectra from the stations (see Figure 6 and Figure 7), this can be explained by the fact that latter was only based on data from two descents of the LOPC, while biovolume spectra from the first transect are based on a lot more data. The reason for not fitting a slope through the whole spectrum is that the spectra showed some signs of nonlinearity out after ~3 mm ESD. Fitting a linear slope through the whole community would then violate the assumption of homoscedasticity, which is important when fitting linear regression. Ignoring these assumptions would lead to biased p-values (Vaughn, 2008). It is also a requirement of biomass spectrum theories that the slope of the spectrum is linear. The fitting of linear models to nonlinear biovolume spectra have been criticized, and using quadratic formulas could improve the fit of the models (Sprules & Barth, 2016).

However, this would lead the models in the study to be incomparable to previous research. Kwong and Pakhomov (2021) has criticized the fitting of slope through a limited size range of the zooplankton community, arguing that the slope and intercept would vary based on the chosen size range.

According to Zhou (2006) a steep slope would indicate highly productive community, as often seen in spring bloom situations. It was therefore unexpected to see a steep slope for the transect of Atlantic Water (see Figure 6), and stations P1 and P6 (see Figure 7), as Atlantic waters had low copepod abundance (~100-250 individuals m^{-2}, see Appendix 3), and mostly lower median egg production rates (see Figure 11), indicating a that copepods of the genus *Calanus* had not cached up to the spring bloom yet.

Moreover, the Arctic station P5 had a relatively flat slope (slope of -0.92, see Figure 7), and high copepod abundance (~1500 individuals m^2, see Appendix 3) as well as high egg production rate (median ~52 eggs $female^{-1}$ day^{-1}, see Figure 12). It is unexpected that the zooplankton community which seems to be in a spring bloom situation based on the net samples, has a flatter slope than the Atlantic community, as theory would predict steep slope for the Arctic station and flat slope in the more dormant Atlantic waters. But the sampling on the Arctic side of the Polar Front was limited to only one station in the present study, so the result should be interpreted with care. It might also be erroneous to make conclusions about the productivity of a community only based on *Calanus spp.* abundance, as small copepods could be equally or more important in terms of production (Basedow et al., 2014). A big contribution to production from small copepods could potentially explain the discrepancy in results obtained from the biovolume spectra and net samples.

The biovolume spectrum based on Arctic influenced water from transect 1 display big similarities the spectrum based on Atlantic water (see Figure 6). As the first transect didn't reach that far north, a better label for Arctic influenced water would probably be Polar Front melt water. The high R^2 values and small error bars for the biovolume spectra presented demonstrate the regularity of the size structure in pelagic zooplankton communities at the Polar Front.

The literature disagrees on what factors determine the slope of the biomass spectrum. Atkinson et al. (2021) emphasize that low trophic transfer efficiency cause a steepening of the

slope, while Zhou (2006) argues that mortality (predation) causes the slope to become steeper. While other authors argue that trophic state of the zooplankton community cannot be inferred from the slope biomass spectrum alone, especially when only a limited portion of the size spectrum is modeled (Kwong, 2021; Noyon et al., 2020). The diverging opinion makes it hard to come to any strong conclusions about the condition of the zooplankton community based on the biovolume spectra alone.

4.3 Estimated growth and secondary production

The estimated growth rate around 0.01-0.02 day^{-1} from the transect seems low, but are plausible and consistent with the literature on *Calanus finmarchicus* growth rates (Kobari et al., 2019). It makes sense that growth rates are on the lower side considering the low temperature on the transects (see Figure 5). It should be mentioned that the empirical formulas the method is based on upon is tailored to copepods and might produce wrong estimates for other taxa of zooplankton. Considering the calibration of the fluorometer, the growth rates could have been overestimated in deep waters and underestimated in the surface.

The estimates of secondary production of on average 5-6 mg C m^{-3} day^{-1} (see Table c) in the surface waters are much smaller than previous estimates done at the Polar front or in the Arctic (Basedow et al., 2014; Trudnowska, Basedow, & Blachowiak-Samolyk, 2014), although the formulas for production differs. One study was done using similar methods and obtained results on a similar scale as the present study: Kwong et al. (2020) estimated secondary production in the Saanich Inlet of British Columbia based on LOPC counts of archived net samples. Sampling was done during all seasons and resulted in estimates of 0.01-18.3 mg C m^{-3} day^{-1} using the Hirst-Bunker growth rate model, which agreed well with the chitobiase method, a method based on moulting enzyme released from crustaceans (Kwong et al., 2020). Considering estimates of primary production from the Barents Sea MIZ during the Spring bloom of 0.5-1.4 g C m^{-2} day^{-1} (Wassmann et al., 1999), the results for secondary production of 5-6 mg C m^{-3} day^{-1} seems plausible and on the right scale.

Although standard errors are low, there is arguably much more uncertainty tied to the parametrization of the growth rate calculations (Chl a concentrations calculated from fluorometer, carbon contents per mg Chl a). The patchiness of areas of high estimated secondary production estimated in the presents study shows the advantage of using semi-automatic sampling techniques applied over a large transect. However, care should be applied when interpreting these estimates of growth and secondary production, as applying semi-empirical growth rate formulas to LOPC measured biovolume is still a novel method.

4.4 Egg production off *Calanus spp.* in relation to total secondary production

Estimated egg contribution to total secondary production in the surface waters was low on the first transect (1.75%), and 5% on the second transect (see Table c). 5% could be considered quite substantial, as it is the egg production of only a single genus. 14% contribution of egg production on transect 2 below the surface layer seems very high. A potential source of error is that all organism of similar size and opacity would be counted as *Calanus* females when basing counts on ESD and AI (Basedow et al., 2013). For example, juvenile krill could be counted as females, this would cause an overestimation of egg production. Considering the vertical migration of krill (Dalpadado et al., 2008), it is not unlikely that the high contribution of egg production in deeper water masses on transect 2 is erroneous. Unfortunately, multinet samples of the zooplankton species composition was not finished by the writing of the present thesis. Data on the species composition would elucidate the results further. Nevertheless, using abundance counts from LOPC to calculate egg production of a single genus or species could still be prone to overestimating egg production, as the potential contribution of some organism of similar size and opacity as the species in question would be hard to rule out.

5 Conclusion

The biovolume spectra from a transect south of the Polar Front displayed steep slopes indicating that the size structure of the community was dominated by small size classes of zooplankton, which according to biomass spectrum theory indicates a productive community, dominated by grazer-predator interactions, with ongoing reproduction fueled by the spring bloom (Zhou, 2006), although other interpretations of the slope exist (Atkinson et al., 2021). The estimates of secondary seems plausible, averaging 5-6 mg C m^{-3} day^{-1} in the upper 50 meters for the two transects south of the Polar Front, but with patches of high production occurred on the second transect (~20-27 mg C m^{-3} day^{-1}). The result from the present paper shows the strength of using towed instrument packages recording environmental and biological data, as spatial patterns of zooplankton production can be discovered. But further validation of this method of calculating growth and production is warranted, to ensure accurate estimates of secondary production. Contribution of *Calanus spp.* egg production to total secondary production was estimated to be 5% in the upper 50 meters, and 14 % in the deeper water on the second transect. But the results might be prone to overestimating egg production as juvenile euphausiids can have a similar size as C. *finmarchicus.* Contribution of *Calanus spp.* egg production to total secondary production on the first transect was estimated to be lower (~1.8% in the upper 50 meters, 4.7% below).

Bibliography

Aarflot, J. M., Skjoldal, H. R., Dalpadado, P., & Skern-Mauritzen, M. (2018). Contribution of Calanus species to the mesozooplankton biomass in the Barents Sea. *ICES Journal of Marine Science, 75*(7), 2342-2354.

Atkinson, A., Lilley, M. K., Hirst, A. G., McEvoy, A. J., Tarran, G. A., Widdicombe, C., . . . Smyth, T. J. (2021). Increasing nutrient stress reduces the efficiency of energy transfer through planktonic size spectra. *Limnology and oceanography, 66*(2), 422-437.

Aune, M., Raskhozheva, E., Andrade, H., Augustine, S., Bambulyak, A., Camus, L., . . . Moiseev, D. (2021). Distribution and ecology of polar cod (*Boreogadus saida*) in the eastern Barents Sea: A review of historical literature. *Marine environmental research, 166*, 105262.

Barton, B. I., Lenn, Y.-D., & Lique, C. (2018). Observed Atlantification of the Barents Sea causes the polar front to limit the expansion of winter sea ice. *Journal of Physical Oceanography, 48*(8), 1849-1866.

Basedow, S. L., Tande, K. S., Norrbin, M. F., & Kristiansen, S. A. (2013). Capturing quantitative zooplankton information in the sea: performance test of laser optical plankton counter and video plankton recorder in a *Calanus finmarchicus* dominated summer situation. *Progress in oceanography, 108*, 72-80.

Basedow, S. L., Tande, K. S., & Zhou, M. (2010). Biovolume spectrum theories applied: spatial patterns of trophic levels within a mesozooplankton community at the polar front. *Journal of Plankton Research, 32*(8), 1105-1119.

Basedow, S. L., Zhou, M., & Tande, K. (2014). Secondary production at the Polar Front. In: Barents.

Berggreen, U., Hansen, B., & Kiørboe, T. (1988). Food size spectra, ingestion and growth of the copepod *Acartia tonsa* during development: implications for determination of copepod production. *Marine Biology, 99*, 341-352.

Blanchard, J. L., Heneghan, R. F., Everett, J. D., Trebilco, R., & Richardson, A. J. (2017). From bacteria to whales: using functional size spectra to model marine ecosystems. *Trends in ecology & evolution, 32*(3), 174-186.

Campbell, R. G., Sherr, E. B., Ashjian, C. J., Plourde, S., Sherr, B. F., Hill, V., & Stockwell, D. A. (2009). Mesozooplankton prey preference and grazing impact in the western Arctic Ocean. *Deep Sea Research Part II: Topical Studies in Oceanography, 56*(17), 1274-1289.

Choquet, M., Kosobokova, K., Kwaśniewski, S., Hatlebakk, M., Dhanasiri, A. K. S., Melle, W., . . . Hoarau, G. (2018). Can morphology reliably distinguish between the copepods *Calanus finmarchicus* and *C. glacialis*, or is DNA the only way? *Limnology and Oceanography: Methods, 16*(4), 237-252.

Daase, M., Berge, J., Søreide, J. E., & Falk-Petersen, S. (2021). Ecology of Arctic Pelagic Communities. *Arctic Ecology*, 219-259.

Dalpadado, P., Arrigo, K. R., Hjøllo, S. S., Rey, F., Ingvaldsen, R. B., Sperfeld, E., . . . Ottersen, G. (2014). Productivity in the Barents Sea-response to recent climate variability. *PLoS one, 9*(5), e95273.

Dalpadado, P., Yamaguchi, A., Ellertsen, B., & Johannessen, S. (2008). Trophic interactions of macro-zooplankton (krill and amphipods) in the Marginal Ice Zone of the Barents

Sea. *Deep Sea Research Part II: Topical Studies in Oceanography, 55*(20-21), 2266-2274.
Espinasse, B., Basedow, S., Schultes, S., Zhou, M., Berline, L., & Carlotti, F. (2018). Conditions for assessing zooplankton abundance with LOPC in coastal waters. *Progress in oceanography, 163*, 260-270.
Falk-Petersen, S., Mayzaud, P., Kattner, G., & Sargent, J. R. (2009). Lipids and life strategy of Arctic *Calanus*. *Marine Biology Research, 5*(1), 18-39.
Fer, I., & Drinkwater, K. (2014). Mixing in the Barents Sea Polar front near Hopen in spring. *Journal of Marine Systems, 130*, 206-218.
Franzè, G., & Lavrentyev, P. J. (2017). Microbial food web structure and dynamics across a natural temperature gradient in a productive polar shelf system. *Marine Ecology Progress Series, 569*, 89-102.
Gallienne, C., Robins, D., & Woodd-Walker, R. (2001). Abundance, distribution and size structure of zooplankton along a 20 west meridional transect of the northeast Atlantic Ocean in July. *Deep Sea Research Part II: Topical Studies in Oceanography, 48*(4-5), 925-949.
Giering, S. L., Wells, S. R., Mayers, K. M., Schuster, H., Cornwell, L., Fileman, E. S., . . . Mayor, D. J. (2019). Seasonal variation of zooplankton community structure and trophic position in the Celtic Sea: A stable isotope and biovolume spectrum approach. *Progress in oceanography, 177*, 101943.
Hatlebakk, M., Kosobokova, K., Daase, M., & Søreide, J. E. (2022). Contrasting life traits of sympatric *Calanus glacialis* and *C. finmarchicus* in a warming Arctic revealed by a year-round study in Isfjorden, Svalbard. *Frontiers in Marine Science, 9*, 673.
Hegseth, E. N. (1998). Primary production of the northern Barents Sea. *Polar Research, 17*(2), 113-123.
Herman, A., Beanlands, B., Chin-Yee, M., Furlong, A., Snow, J., Young, S., & Phillips, T. (1998). The Moving Vessel Profiler (MVP): In-situ sampling of plankton and physical parameters at 12 kts and the integration of a new laser/optical plankton counter. *Oceanology, 102*, 123-135.
Herman, A., Beanlands, B., & Phillips, E. (2004). The next generation of optical plankton counter: the laser-OPC. *Journal of Plankton Research, 26*(10), 1135-1145.
Hirche, H.-J., & Bohrer, R. (1987). Reproduction of the Arctic copepod Calanus glacialis in Fram Strait. *Marine Biology, 94*, 11-17.
Hirst, A., & Bunker, A. (2003). Growth of marine planktonic copepods: global rates and patterns in relation to chlorophyll a, temperature, and body weight. *Limnology and oceanography, 48*(5), 1988-2010.
Huntley, M., & Boyd, C. (1984). Food-limited growth of marine zooplankton. *The American Naturalist, 124*(4), 455-478.
Huntley, M. E., & Lopez, M. D. (1992). Temperature-dependent production of marine copepods: a global synthesis. *The American Naturalist, 140*(2), 201-242.
Kobari, T., Sastri, A. R., Yebra, L., Liu, H., & Hopcroft, R. R. (2019). Evaluation of trade-offs in traditional methodologies for measuring metazooplankton growth rates: assumptions, advantages and disadvantages for field applications. *Progress in oceanography, 178*, 102137.
Kortsch, S., Primicerio, R., Fossheim, M., Dolgov, A. V., & Aschan, M. (2015). Climate change alters the structure of arctic marine food webs due to poleward shifts of boreal generalists. *Proceedings of the Royal Society B: Biological Sciences, 282*(1814), 20151546.

Kvile, K. Ø., Fiksen, Ø., Prokopchuk, I., & Opdal, A. F. (2017). Coupling survey data with drift model results suggests that local spawning is important for Calanus finmarchicus production in the Barents Sea. *Journal of Marine Systems, 165*, 69-76.
Kwong, L. E. (2021). *Mesozooplankton normalized biomass size spectra and production in the northeast Pacific.* University of British Columbia,
Kwong, L. E., & Pakhomov, E. A. (2021). Zooplankton size spectra and production assessed by two different nets in the subarctic Northeast Pacific. *Journal of Plankton Research, 43*(4), 527-545.
Kwong, L. E., Suchy, K. D., Sastri, A. R., Dower, J. F., & Pakhomov, E. A. (2020). Comparison of mesozooplankton production estimates from Saanich inlet (British Columbia, Canada) using the chitobiase and biomass size spectra approaches. *Marine Ecology Progress Series, 655*, 59-75.
Mehner, T., Lischke, B., Scharnweber, K., Attermeyer, K., Brothers, S., Gaedke, U., . . . Brucet, S. (2018). Empirical correspondence between trophic transfer efficiency in freshwater food webs and the slope of their size spectra. *Ecology, 99*(6), 1463-1472.
Noyon, M., Rasoloarijao, Z., Huggett, J., Ternon, J.-F., & Roberts, M. (2020). Comparison of mesozooplankton communities at three shallow seamounts in the South West Indian Ocean. *Deep Sea Research Part II: Topical Studies in Oceanography, 176*, 104759.
Ohman, M. D., & Runge, J. A. (1994). Sustained fecundity when phytoplankton resources are in short supply: omnivory by Calanus finmarchicus in the Gulf of St. Lawrence. *Limnology and oceanography, 39*(1), 21-36.
Orlova, E. L., Rudneva, G. B., Renaud, P. E., Eiane, K., Savinov, V., & Yurko, A. S. (2010). Climate impacts on feeding and condition of capelin *Mallotus villosus* in the Barents Sea: evidence and mechanisms from a 30 year data set. *Aquatic Biology, 10*(2), 105-118.
Platt, T., & Denman, K. (1977). Organisation in the pelagic ecosystem. *Helgoländer Wissenschaftliche Meeresuntersuchungen, 30*, 575-581.
Poulet, S., Ianora, A., Laabir, M., & Breteler, W. K. (1995). Towards the measurement of secondary production and recruitment in copepods. *ICES Journal of Marine Science, 52*(3-4), 359-368.
R Core Team. (2022). R: A language and environment for statistical computing. Vienna, Austria.: R Foundation for Statistical Computing.
Reigstad, M., Wassmann, P., Riser, C. W., Øygarden, S., & Rey, F. (2002). Variations in hydrography, nutrients and chlorophyll a in the marginal ice-zone and the central Barents Sea. *Journal of Marine Systems, 38*(1-2), 9-29.
Runge, J., & Roff, J. (2000). The measurement of growth and reproductive rates. In *ICES zooplankton methodology manual* (pp. 401-454): Elsevier.
Sheldon, R., Prakash, A., & Sutcliffe Jr, W. (1972). The size distribution of particles in the ocean. *Limnology and oceanography, 17*(3), 327-340.
Skaret, G., Dalpadado, P., Hjøllo, S. S., Skogen, M. D., & Strand, E. (2014). Calanus finmarchicus abundance, production and population dynamics in the Barents Sea in a future climate. *Progress in oceanography, 125*, 26-39.
Sprules, W. G., & Barth, L. E. (2016). Surfing the biomass size spectrum: some remarks on history, theory, and application. *Canadian Journal of Fisheries and Aquatic Sciences, 73*(4), 477-495.
Trudnowska, E., Basedow, S. L., & Blachowiak-Samolyk, K. (2014). Mid-summer mesozooplankton biomass, its size distribution, and estimated production within a glacial Arctic fjord (Hornsund, Svalbard). *Journal of Marine Systems, 137*, 55-66.

Våge, S., Basedow, S., Tande, K., & Zhou, M. (2014). Physical structure of the Barents Sea Polar Front near Storbanken in August 2007. *Journal of Marine Systems, 130*, 256-262.
Vaughn, B. K. (2008). Data analysis using regression and multilevel/hierarchical models. In: JSTOR.
Vincent, W. F. (2010). Microbial ecosystem responses to rapid climate change in the Arctic. *The ISME journal*, *4*(9), 1087-1090.
Wassmann, P., Ratkova, T., Andreassen, I., Vernet, M., Pedersen, G., & Rey, F. (1999). Spring bloom development in the marginal ice zone and the central Barents Sea. *Marine Ecology, 20*(3‐4), 321-346.
Wickham, H. (2016). ggplot2: Elegant Graphics for Data Analysis. New York: Springer-Verlag
Wickham, H., François, R., Henry, L., & Müller, K. (2015). dplyr: A grammar of data manipulation. *R package version 0.4*, *3*, p156.
Zhou, M. (2006). What determines the slope of a plankton biomass spectrum? *Journal of Plankton Research, 28*(5), 437-448.
Zhou, M., Carlotti, F., & Zhu, Y. (2010). A size-spectrum zooplankton closure model for ecosystem modelling. *Journal of Plankton Research, 32*(8), 1147-1165.
Zhou, M., & Huntley, M. E. (1997). Population dynamics theory of plankton based on biomass spectra. *Marine Ecology Progress Series*, *159*, 61-73.
Zhou, M., Tande, K. S., Zhu, Y., & Basedow, S. (2009). Productivity, trophic levels and size spectra of zooplankton in northern Norwegian shelf regions. *Deep Sea Research Part II: Topical Studies in Oceanography*, *56*(21-22), 1934-1944.

Appendix

Appendix 1: LOPC size classes, in mm^3 ESD, log10 (mm^3), as plotted on the biovolume spectra, as well as interval width.

Start of size class, mm^3	ESD	Log10(mm^3)	Size interval Δv, mm^3
5.25E-04	0.1	-3.28	2.17E-04
7.41E-04	0.112	-3.13	3.06E-04
1.05E-03	0.126	-2.98	4.32E-04
1.48E-03	0.141	-2.83	6.10E-04
2.09E-03	0.159	-2.68	8.62E-04
2.95E-03	0.178	-2.53	1.22E-03
4.17E-03	0.2	-2.38	1.72E-03
5.89E-03	0.224	-2.23	2.43E-03
8.32E-03	0.251	-2.08	3.43E-03
0.01175	0.282	-1.93	0.005
0.0166	0.316	-1.78	0.007
0.02344	0.355	-1.63	0.010
0.03311	0.398	-1.48	0.014
0.04677	0.447	-1.33	0.019
0.06607	0.502	-1.18	0.027
0.09333	0.563	-1.03	0.038
0.1318	0.631	-0.88	0.054
0.1862	0.708	-0.73	0.077
0.263	0.795	-0.58	0.11
0.3715	0.892	-0.43	0.15
0.5248	1.001	-0.28	0.22
0.7413	1.123	-0.13	0.31
1.047	1.26	0.02	0.43
1.479	1.414	0.17	0.61
2.089	1.586	0.32	0.86
2.951	1.78	0.47	1.2
4.169	1.997	0.62	1.7
5.888	2.24	0.77	2.4
8.318	2.514	0.92	3.4
11.75	2.821	1.07	4.9
16.6	3.165	1.22	6.8
23.44	3.551	1.37	9.7
33.11	3.984	1.52	13.7
46.77	4.47	1.67	19.3
66.07	5.016	1.82	27.3
93.33	5.628	1.97	38.5
131.8	6.314	2.12	54.4
186.2	7.085	2.27	76.8
263	7.949	2.42	108.5
371.5	8.919	2.57	153.3
524.8	10.008	2.72	216.5
741.3	11.229	2.87	305.7
1047	12.599	3.02	432

1479	14.136	3.17	610
2089	15.861	3.32	862
2951	17.796	3.47	1000
4169	19.968	3.62	1218
5888	22.404	3.77	1719
8318	25.138	3.92	2430

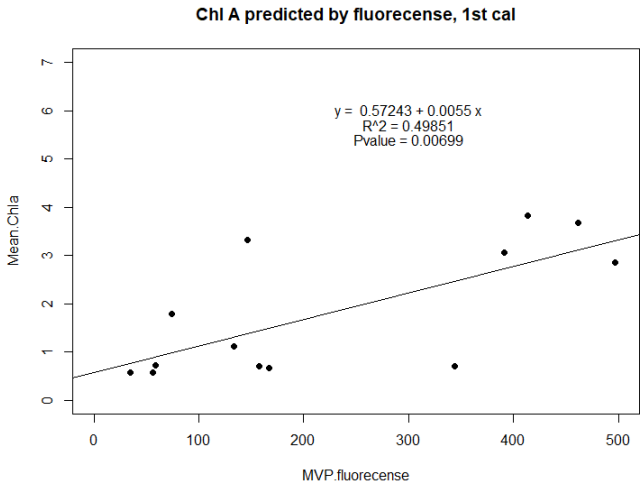

Appendix 2: Fluorescence calibration with filtration.

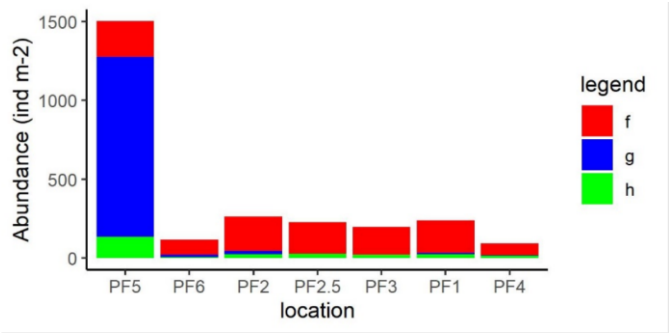

Appendix 3: Abundance of Calanus spp. individuals sampled with WP3 (WP2 at station 6), arranged by station, according to latitude (from North to south), figure courtesy of M. Daase.